Available online at www.sciencedirect.com

SciVerse ScienceDirect

Procedia Engineering 00 (2015) 000–000

SAND2014-18754C

Procedia Engineering

www.elsevier.com/locate/procedia

The 13th Hypervelocity Impact Symposium

Computational modeling of electrostatic charge and fields produced by hypervelocity impact

David A. Crawford*

Sandia National Laboratories, P. O. Box 5800, MS 0840, Albuquerque, NM 87185*

Abstract

Following prior experimental evidence of electrostatic charge separation, electric and magnetic fields produced by hypervelocity impact, we have developed a model of electrostatic charge separation based on plasma sheath theory and implemented it into the CTH shock physics code. Preliminary assessment of the model shows good qualitative and quantitative agreement between the model and prior experiments at least in the hypervelocity regime for the porous carbonate material tested. Moreover, the model agrees with the scaling analysis of experimental data performed in the prior work, suggesting that electric charge separation and the resulting electric and magnetic fields can be a substantial effect at larger scales, higher impact velocities, or both.

Keywords: magnetic field, electric field, plasma, hypervelocity impact

1. Introduction

In prior work with experiments performed at the NASA Ames Vertical Gun Range (AVGR), electrostatic charge separation during hypervelocity impact was characterized for different impactor and target geometries [1]. The experiments directly measured the charge ejected at early time from craters produced by vertical impacts. An array of aluminum plates detected charge arrival as a function of angle of ejection from the target surface. Total charge separation was found to vary nearly linearly with mass and possessed a velocity dependence of $v^{2.6\pm0.1}$ (Fig. 1). Extrapolating these observations using a simple dipole assumption with a characteristic length scale (x) and corresponding time scale (τ), Crawford and Schultz [1] showed the magnitude and duration of the electric field (E), electric current (I) and magnetic field (B) for several cases: 1) laboratory experiment (m=2x10^{-4} kg, x=0.5 m, v=5 km/s), 2) Leonid meteoroid (m=10^{-7} kg, x=1 m) striking a spacecraft at 72 km/s, 3) small meteoroid (m=1 kg, x=3 m) striking the Moon at 15 km/s and 4) 1 km asteroid (m=10^{12} kg, x=100 km) striking a planetary surface at 20 km/s (Table 1).

Table 1. Electromagnetic properties of representative impacts, from [1].

	τ (sec.)	E (Volts/m)	I (Amps)	B (Tesla)
1) Laboratory	2x10^{-3}	8x10^{5}	4x10^{-3}	10^{-9}
2) Leonid Meteoroid	3x10^{-4}	10^{5}	0.02	10^{-8}
3) Small Meteoroid	4x10^{-3}	2x10^{9}	180	10^{-5}
4) 1 km Asteroid	100	4x10^{12}	2x10^{10}	0.03

* Corresponding author. Tel.: 1-505-221-8288.
E-mail address:dacrawf@sandia.gov.

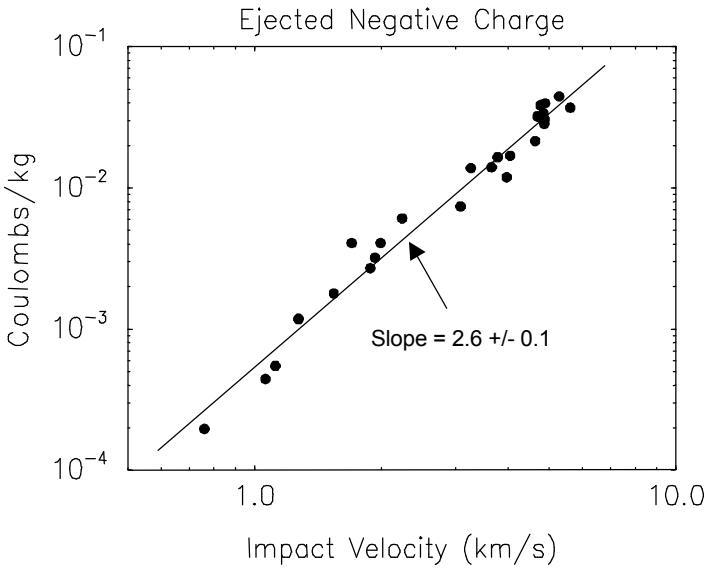

Fig. 1. Negative charge per unit projectile mass ejected by impacts of spherical aluminum projectiles into granular carbonate (dolomite) targets vs. impact velocity, from [1].

2. Model

In an attempt to better understand the formative mechanism of electrostatic charge separation during hypervelocity impacts and provide a closer-to-first principles predictive capability, we have developed a model based on plasma sheath theory which we have incorporated into the CTH shock physics code [2].

Hypervelocity impact produces weakly ionized gas, solid and liquid (condensed phase) fragments. Due to the substantial mass difference between ions and much lighter electrons, electrons more frequently collide with and stick to condensed phase surfaces until a negative potential develops that impedes further deposition of electrons. The relative motion of plasma and condensed phases produces separation of electrostatic charge over macroscopic distances leading to the generation of electrostatic and magnetostatic fields. We now believe these fields to be the source of signals seen in earlier hypervelocity impact experiments conducted at the AVGR [3,4,5].

In our model, we track gas phases and condensed phases separately using different CTH material IDs. Mass is exchanged between the gas and condensed phases of a given material whenever the material temperature transitions above or below a vaporization temperature (T_v) provided by user input. Even at modest temperature of just a fraction of an electron volt (a few thousand °K), the gas phase will be a weakly ionized gas containing free electrons (N_e) and ions (N_i) constrained by the Saha Equation [6]:

$$N_i = \left(N_k \frac{Z_i}{Z} \right)^{1/2} \left(\frac{2\pi m_e kT}{h^2} \right)^{3/4} e^{-E_i/2kT} \tag{1}$$

where: N_k (cm^{-3}) is neutral number density (N_k=$N_0 \cdot m$, with m, the mass of substance), E_i (eV) is ionization energy and Z_i/Z ~o(1) is the ratio of partition functions. Initially, free electrons and ions are in local equilibrium maintaining charge neutrality even at microscopic scale. However, the condensed phase may collect charge from collision of ions and electrons at the interface with ionized gas phases. Initial charge separation distance is governed by the Debye Length, $\lambda_d=(\varepsilon_0 kT/N_e e^2)^{1/2}$; however, hydrodynamic motion can separate the phases, thereby leading to macroscopic charge separation. Collision rates are determined by ion (J_i) and electron (J_e) thermal currents that in turn depend on gas phase temperature, ion and electron concentrations:

$$J_i = \frac{N_i}{4} \left(\frac{kT}{\pi m_i} \right)^{1/2} \tag{2}$$

$$J_e = \frac{N_e}{4}\left(\frac{kT}{\pi m_e}\right)^{1/2} \exp\left(-\frac{e\phi_0}{kT}\right) \tag{3}$$

Where N_e is the local electron density, m_e and m_i are the mass of the electron and dominant ion respectively, and ϕ_0 is the electrostatic potential on the surface of the condensed phase. We can determine the equilibrium potential (ϕ_e) at the surface of condensed phase materials by equating J_i and J_e:

$$\phi_0 = \phi_e = \frac{kT}{e}\ln\left(\frac{m_i}{m_e}\right)^{1/2} \tag{4}$$

which implies an equilibrium surface charge (Q_e) of:

$$Q_e = -\frac{\phi_e\sqrt{2}}{\varepsilon_0\lambda_D}A \tag{5}$$

where A is the local surface area of the condensed phase materials.

In our numerical model, we calculate surface charge (Q_s) by explicitly integrating Equations (2) and (3) in computational cells that contain an interface between condensed phases and ionized gases. In the present version of the model, we consider only positive singly charged ions (always constrained by Equation 1) and free electrons. Under these circumstances J_i acts to increase Q_s and J_e acts to decrease Q_s. We limit the integration to the equilibrium surface charge (Q_e) when the thermal currents would otherwise drive Q_s past the equilibrium value. However, charge can reach a "frozen" condition when temperature and/or ion density of the gas phase drops faster than thermal currents can act to preserve equilibrium, either by moving away from the equilibrium value or not moving fast enough towards it. Overall charge neutrality is maintained via constraint equations applied to the condensed-phase bound charge and gas-phase free electrons. The local ion density is always in thermodynamic equilibrium with the neutral gas atoms via Equation (1).

The surface area (A) of condensed phases in a computational cell is approximated by:

$$A = \left[\frac{M\min\left(4\pi L_p^2, A_{cell}\right)}{\rho_{ref}\min\left(\frac{4}{3}\pi L_p^3, V_{cell}\right)}\right] \tag{6}$$

where M is the mass of the condensed phases in the cell, L_p is the particle size (from user input), ρ_{ref} is the reference density of the condensed phase (STP conditions) and V_{cell} is the cell volume, with $A_{cell} = V_{cell}/\Delta x$ a representative cell cross-section.

Figure 2 shows a simulation of a 0.64 cm spherical aluminum projectile vertically striking a porous calcite target at 5 km/s. For this simulation, we used the electrostatic charge separation model with properties shown in Table 2. The projectile was modeled using the ANEOS equation-of-state (EOS) for aluminum, a SESAME calcite EOS with 26% porosity modeled using the P-Alpha model and a SESAME air EOS. Because of the strong temperature dependence of Equation (1) use of a good EOS is critical.

Table 2. Parameters used in the CTH electrostatic charge model.

	Aluminum	Air	Calcite
N_0 (g^{-1})	2.23×10^{22}	4×10^{20}	6×10^{21}
E_i (eV)	5.99	9.26	6.11
Z_i / Z	0.17	1	1.74
m_i (amu)	26.98	30	40
T_v (eV)	0.24	0	0.09
L_p (cm)	0.01	N/A	0.05

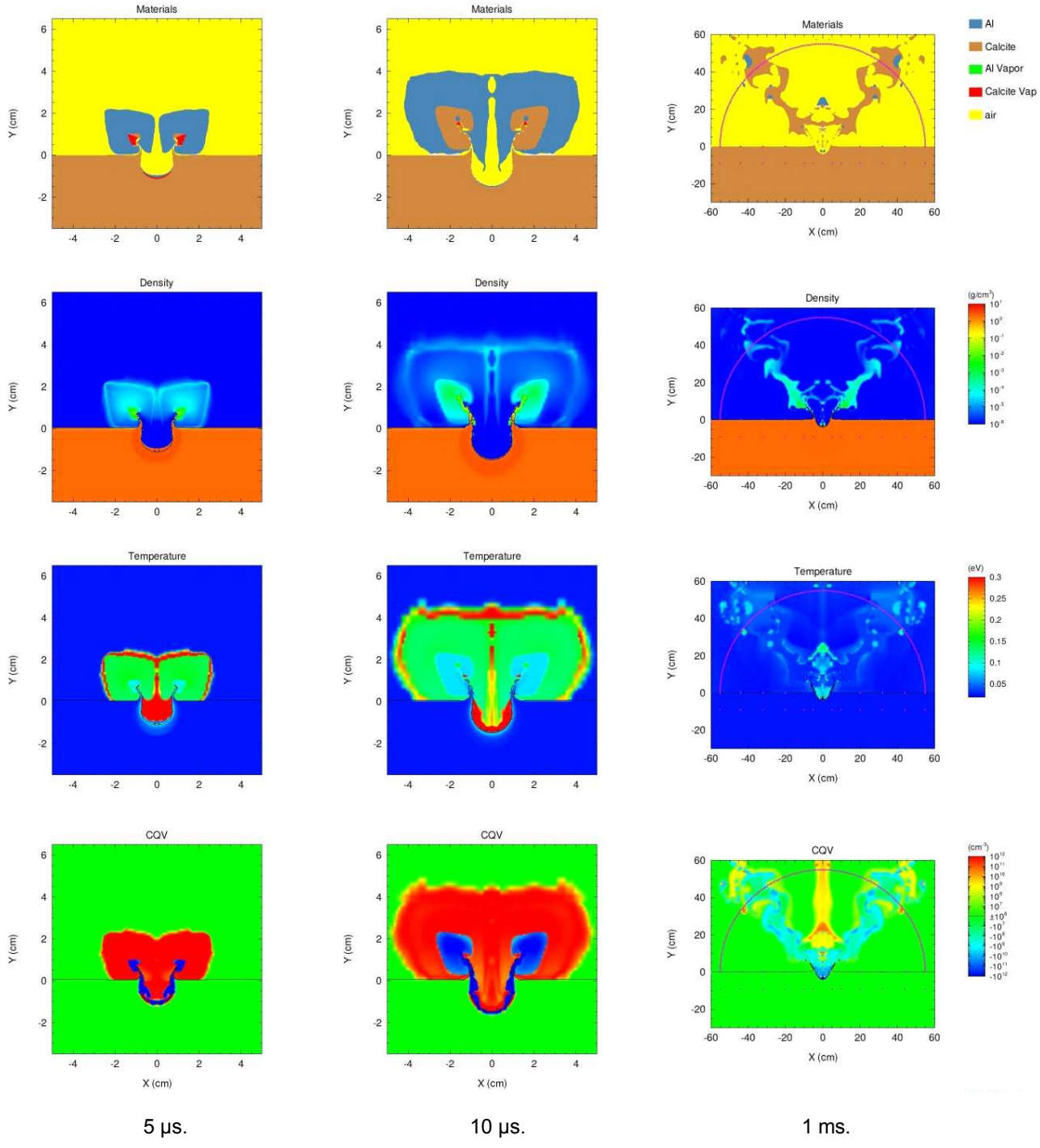

Fig. 2. CTH simulation of the vertical impact of a 0.64-cm spherical aluminum projectile into a calcite target at 5 km/s using the electrostatic charge separation model. The calcite target has a porosity of 26%. Even though the experiment was conducted in a vacuum of approximately 1 mbar, the residual air can still contribute ionization and must be accounted for. At this velocity, aluminum never vaporizes. Some of the calcite decomposes into CO_2 and CaO at approximately 1,000 °K. (The CaO can re-condense yet the CO_2 remains a gas.) Bottom sequence shows the net electrostatic charge density (CQV) in number of protons (or electrons) per unit volume. Air and aluminum tend to acquire positive charge (red) whereas calcite tends to acquire negative charge (blue). Currents collected on the charge sensor plates (indicated by the arc at 55 cm radius) reflect the distribution seen here (Fig. 3).

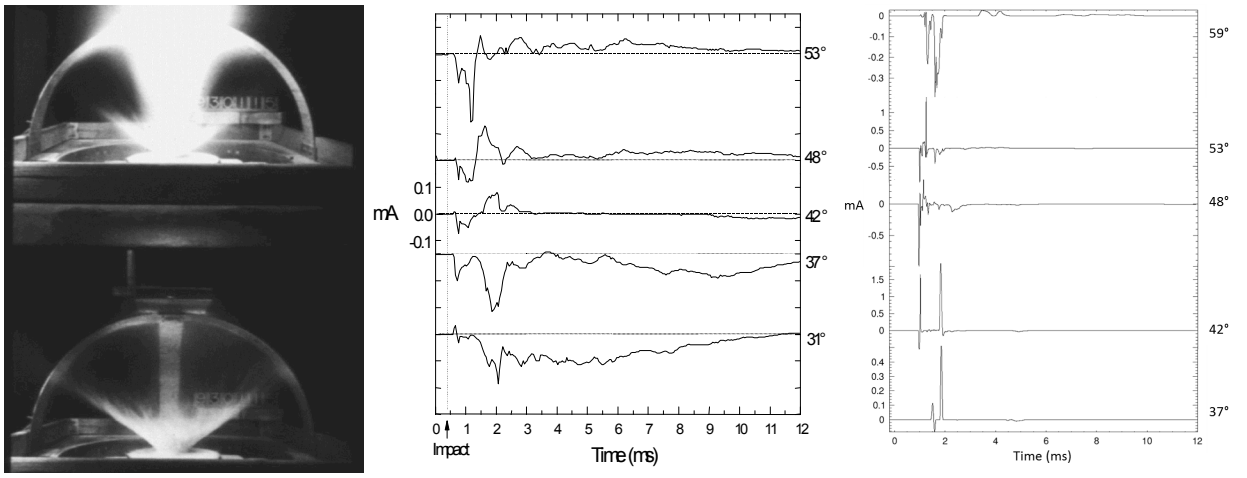

Fig. 3. (Left) Two movie frames from an experiment designed to measure charge ejected from an impact in a particulate carbonate target, from [1]. The projectile was a 0.48 cm aluminum sphere impacting at 5 km/s in an evacuated target chamber. The upper frame shows luminescent material impinging on the upper portion of an arc of 16 charge detection plates. The lower frame, 2 ms later, shows ejecta hitting the arc at 35 degrees. The radius of the arc is 55 cm. (Center) Electric current collected by probes located on the arc. Each probe's ejection angle is shown. (Right) CTH simulation of the currents collected at plates covering a similar range in ejection angles.

a) Photograph of experimental setup

b) Experimental measurements

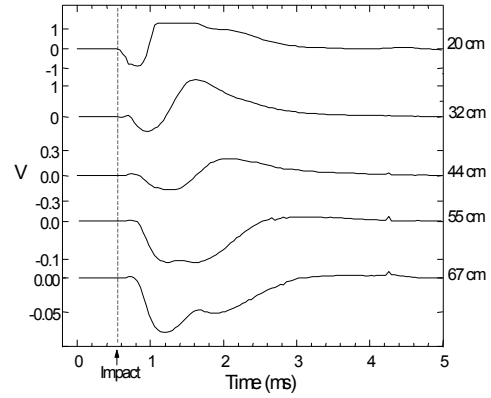

c) CTH simulation

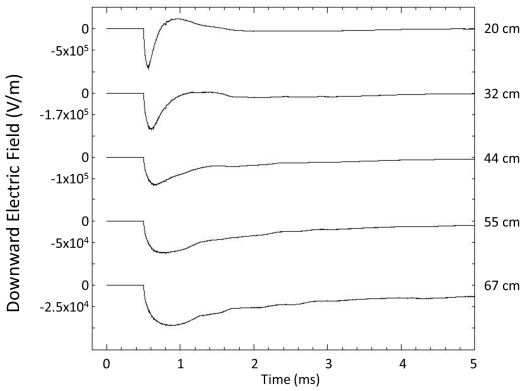

Fig. 4. Experiment to measure the electrostatic field produced by the impact of a 0.64 cm aluminum projectile into a particulate carbonate target (impact velocity: 5 km/s, vertical), from [1]. a) The impact crater (10 cm diameter) can be seen in the foreground and several of the plates located 20 and 32 cm from the impact are shown in the background. b) The voltage measured on plates distributed radially from the impact point is shown with distance from the center of the impact crater indicated. c) CTH simulation of the downward component of the electric field (V/m) at the same experimental locations and shifted in time to correspond to the experimental impact time of ~0.5 ms.

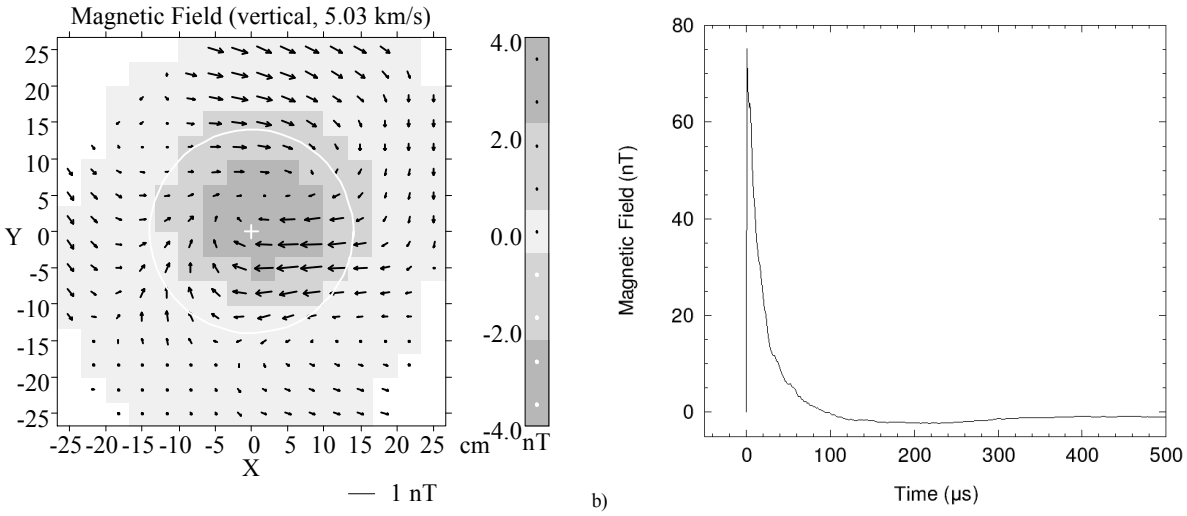

Fig. 5. a) Transient magnetic field observed in a low initial magnetic field environment (500 nT oriented vertically—up) 0.1-0.3 ms after vertical hypervelocity (~5 km/s) impacts of 0.64 cm aluminum projectiles into a powdered dolomite target, from [5]. The plot is the average of several impact experiments (75 measurement locations/orientations) with each measurement located in a horizontal plane 9 cm below the impact point. Shading represents the vertical component of the magnetic field whereas vectors represent the horizontal. The crater (white circle) defines the origin (white cross) of the coordinate system. b) Magnetic field strength computed by CTH with model described in the text. The field prediction is for a location 9 cm below and at a radius of 20 cm from the impact location. The field is toroidal, consistent with being generated by a vertically oriented electric current, initially oriented upward for the first 100 μs, followed by a weaker, but longer lasting downward current system (i.e. negative charge moving upward). The average field of about -2 nT from 100-300 μs is consistent with the experimental observations shown on the left.

3. Results

While not in perfect agreement, CTH simulation results show good qualitative agreement with the spatial and temporal charge distribution seen during the impact experiments. Figure 3 shows an experiment conducted by Crawford and Schultz [1] to measure the electric charge produced during a hypervelocity impact into porous calcite. An array of 16 charge detection plates were placed to measure electric charge arrival at 16 different ejection angles. The electric currents predicted by the simulation show good qualitative agreement with the experimentally measured values, having similar bimodal signatures and comparable magnitudes. The electric and magnetic fields predicted by the model also show good agreement with the experimental values (Figures 4 and 5).

Furthermore, the overall charge state predicted by the model agrees *quantitatively* with the experimental data of Figure 1. The model matches the linear mass dependence and the strong velocity dependence of the experimental data at least in the carbonate vaporization/ionization regime (Figure 6). Substantial disagreement between the model and experimental data occurs below impact velocities of about 2 km/s. The cause of this is unknown. The only ionization mechanism operating in the model in this velocity range is from air, with NO^+ the dominant ion. We can speculate that the P-Alpha model is inadequate to describe calcite vaporization at low velocities. It wouldn't be too hard to imagine that hot spots formed from pore collapse may be occurring in the calcite at the micro-scale (something not expected to be accurately represented by the P-Alpha model). At velocities higher than about 8 km/s, the model predicts aluminum vaporization will begin to contribute ions, producing a substantial increase in electric charge production (Figure 6). This would be a reasonable prediction of the model for future experimental tests.

4. Conclusions and Future Directions

We have developed a model of electrostatic charge separation based on plasma sheath theory and implemented it into the CTH shock physics code. Preliminary assessment of the model shows good qualitative and quantitative agreement between the model and prior experiments at least in the hypervelocity regime for the porous carbonate material tested. Moreover, the model agrees with the scaling analysis of experimental data performed in prior work [1], suggesting that electric charge separation and the resulting electric and magnetic fields can be a substantial effect at larger scales, higher impact velocities, or both. In future work, we will explore the implications of this model for the paleomagnetic record of cratered planetary and small body surfaces in the solar system.

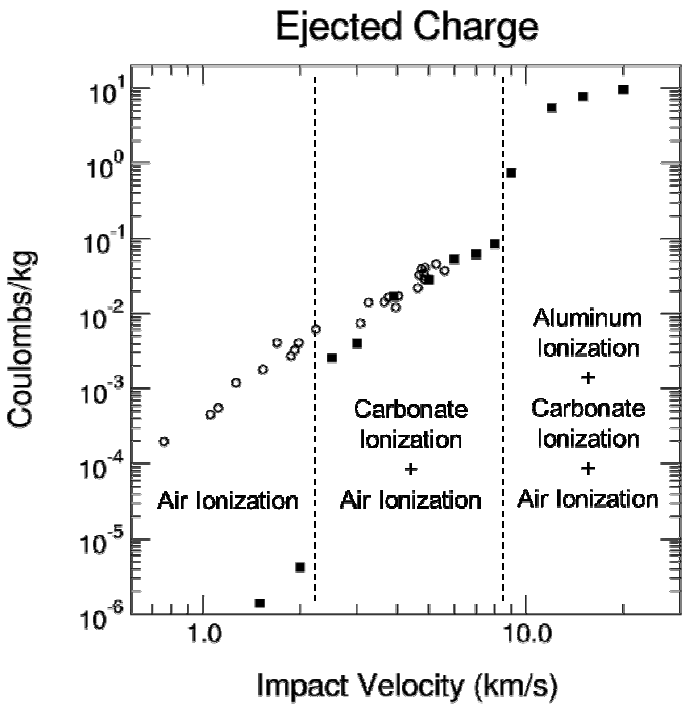

Fig. 6. Total negative charge per unit mass ejected vs. impact velocity. Experimental results from [1] are shown with open black circles. CTH simulation results using the model described in the text are shown with solid black squares. Good agreement between experiments and simulations is seen in the carbonate vaporization (and ionization) regime. The lack of agreement at low velocities, where simulations predict only air ionization to contribute, is discussed in the text.

Acknowledgements

Sandia is a multiprogram laboratory operated by Sandia Corporation, a Lockheed Martin Company, for the United States Department of Energy under Contract DE-AC04-94AL85000.

References

[1] Crawford, D. A., Schultz, P. H., 1999, Electromagnetic Properties of Impact-Generated Plasma, Vapor and Debris, International Journal of Impact Engineering, 23, pp. 169-180.
[2] McGlaun, J. M, Thompson S. L., Elrick, M. G., 1990, CTH - A Three-Dimensional Shock-Wave Physics Code, International Journal of Impact Engineering, 10, p. 351.
[3] Crawford, D. A., Schultz, P. H., 1988, Laboratory observations of impact–generated magnetic fields, Nature, 336, pp. 50-52.
[4] Crawford, D. A., Schultz, P. H., 1991, Laboratory Investigations of Impact-Generated Plasma, Journal of Geophysical Research, Vol. 96, No. E3, pp. 18,807-18,817.
[5] Crawford, D. A., Schultz, P. H., 1993, The production and evolution of impact-generated magnetic fields, International Journal of Impact Engineering, 14, pp. 205-216.
[6] Saha, M. N., 1920, Ionisation in the Solar Chromosphere, Philosophical Magazine, 40, October, 1920.